Scattering Spectroscopy of Plasmonic Janus Particles

Felix H. Patzschke, A. Markus Anton and *Frank Cichos

Abstract

Plasmonic Janus particles consist of dielectric core particles with a thin metallic cap on one side and are widely used in active matter research. [1] The plasmonic cap enhances optical scattering and absorption, allowing for self-propulsion through temperature gradients as well as efficient trapping and tracking. [2, 3] The asymmetry of such a particle gives rise to surface plasmon modes whose excitation is sensitive to the angle at which the particle is illuminated. Even though the angle of illumination strongly influences the particle's scattering response, the optical properties of such metallic caps have hardly been investigated.

We probe the light scattering of individual micrometre-sized, spherical, Au-coated Janus particles by means of Selective Illumination Multiplexed Fourier Plane Spectroscopy. This novel method allows us to explore microparticles' scattering characteristics resolved for wavelength, angle of illumination and scattering angle.

In addition, we supplement our experimental results with finite-element simulations and correlate spectral markers to orientation-dependent surface plasmon modes. This additional information on the correlation of angular and spectral information could pave the way for new methods of orientation detection. They also shed new light on the interaction of such spherically capped particles with light inducing forces and torques. [4, 5]

Introduction

Janus particles (JPs) with a plasmonically active cap are a widely-used tool in active matter research: Through the absorption of visible light, the cap can be heated efficiently. In conjunction with the anisotropy of the particle, this facilitates directed self-propulsion. Meanwhile, the enhanced optical scattering of the cap leads to good visibility in microscopy, particularly in the dark field, which, in turn, allows for accurate tracking of the motile particles.

[However, orientation studies are usually performed in 2D, as ...]

As widely applicable as these particles' light-matter interactions (LMIs) may be, the are certainly not trivial: The length scales of the surface curvature are in the same order of magnitude as the wavelengths of light in the interaction, such that approximations along the lines of ray optics or dipole scattering are invalid. In addition, the asymmetry of the particles leads to orientation-dependency of the LMI. These orientation-dependencies may manifest in counter-intuitive ways: Some purely numerical studies suggest that plasmonic JPs can stably rotate, powered by a linearly polarized light field. [4, 5]

As a first step towards an understanding of such effects, we study the scattered light from these JPs. We measure scattering spectra of individual JPs while varying the direction of illumination as well as resolving for the scattering angle. While orientation-dependent scattering studies of plasmonic nanostructures *have* been performed, [6] that has only been the case for Au nanostructures significantly smaller than the observation wavelengths. As such, no regard was given to the angular distribution of the scattered light. In our studies of micrometre-sized JPs in visible and NIR light though, we find that the difference in shape of these distributions can lead to drastic, qualitative differences in measured scattering spectra.

We present an experimental method, which we use to study the LMI of plasmonic JPs consisting of a spherical polystyrene (PS) particle, 1 µm in diameter, with a 50 nm thick gold layer as the cap. We resolve the intensity of scattered light for wavelength and scattering angle. Though the theory of Mie [7] only makes predictions for maximally symmetric particles, it serves well as reference in the characterization of the LMI of plasmonic JPs.

We complement the measurement results with numerical simulations and find a good match between both methods' results. Through the analysis of the simulation results, we correlate peaks in the scattering spectra to orientation-dependent surface plasmon modes.

Definitions

[Introduction of the real, physical sample: Mathematical formalization should go after.]

The geometry of the system of interest is as follows: A polystyrene (PS) sphere ($r = 0.5\,\mu m$), centered at the origin, represents the core of the JP. The gold cap is modelled as half of an ellipsoidal shell (semi major axis: 0.55 µm, semi minor axes: 0.51 µm) around the PS sphere. It is cut off in the plane of the minor axes, its major axis coincides with the symmetry axis of the JP. This construct is surrounded by an ambient medium with a constant, real-valued refractive index.

The orientation of the system is characterised by the angles between three unit vectors;

$\hat{z}$, the symmetry axis of the particle, oriented such that the Au cap lies in the positive and the PS side in the negative z-direction,

$\hat{k}$, the propagation direction of the incident light, with respect to which scattering angles are defined and

$\hat{o}$, the "forward" direction along the optical axis, equivalent to the central axis of the objective's collection cone.

In terms of these, the out-of-plane orientation of the JP is defined as $\alpha := \measuredangle(\hat{o}, \hat{z})$. Similarly, we define the illumination angle $\zeta := \measuredangle(\hat{k}, \hat{z})$, which, in this model, is the only orientation parameter needed to define the light-matter interaction of the JP.

Scattering angles are defined for each plane-wave contribution to the scattered field: Let that contribution have a propagation direction $\hat{k}'$. Then, $\theta := \measuredangle(\hat{k}', \hat{k})$ is the polar component of the scattering angle. Additionally, there is an azimuthal component ϕ, the choice of reference point for which being somewhat arbitrary. In the following, it will be chosen such that if $\hat{k}'$ lies in the $(\hat{k}, \hat{z})$ plane, then $\phi = 0$.

These definitions are illustrated in [Figure] .

Methods

Experiments

Sample Preparation

The JPs were produced by [cite production from Nic's work] and consist of spherical PS beads, coated with a layer of gold, 50 nm thick on average, on one side, with a 5 nm thick layer of chromium as a binding agent in between. A 30 µl droplet was placed on a cover slip and the JPs in solution were left to sediment for 10 minutes. Afterwards, the solvent was blown off using nitrogen gas, leaving the remaining JPs stuck on the coverslide. A second cover slip was placed on top, with a droplet of 1.5 µl of immersion oil[1] in between, such as to keep the ambient refractive index constant in the vicinity of the particles.

Optical Setup

The imaging setup is sketched in Figure 1C. Its basis was formed by a standard dark-field microscope. A confocal aperture in the image plane of the dark-field microscope was used to isolate the scattered light from a single particle. A homebuilt spectrograph was used to extract spectral information from the microscope image. It consisted of

- an sCMOS camera (pco.edge 4.2) for image acquisition,

(G) a transmissive diffraction grating (ThorLabs GTI25-03A) in front of it, used for spectral dispersal of the image,

(A5) a tunable slit to select only a thin vertical line from an image in order to prevent overlap of spectrally dispersed signals from different points in the original image and

- a lens to propagate the image from the plane of the slit onto the camera sensor.

Both sub-assemblies were linked by a propagating optic, with which either the image plane wherein the aperture lay or the back focal plane (BFP) of the microscope objective could be chosen to be projected onto the slit.

The real-space-imaging mode was used to select particles for measurement as well as for spectral measurements in which the scattering angle was not resolved. The BFP-imaging mode was used to align the dark-field illumination and to record spectrally resolved Fourier-space images of the JP under observation. To that end, the front aperture of the spectrograph (i.e. the slit A5) was slowly translated across the BFP image while recording, such that the camera would record one spectrally dispersed vertical line of the BFP image at a time. The accumulation time for one such dataset was approximately 15 minutes.

Measurements had to be corrected for the spectral response function of the setup. This was recorded by opening the objective's back aperture (A3) fully, allowing the illumination light to pass through the entire assembly.

Validation

For validation, the scattering spectra of 65 nm AuNPs were measured. Such small particles were chosen for two reasons: a) The resonance in the expected scattering spectrum would be as narrow as possible and b) the shape of the angular distribution of scattered light would not change appreciably over the spectral range of interest, causing the measured and full scattering cross-sections to only differ by a constant factor. In the comparison of the measured spectra to the predictions of Mie theory [7–9] using the values by Johnson & Christy [10] for the complex refractive index of gold shows a strong agreement.

We find a good match between the measured and theoretical spectra. This is, in part, due to our choice of particles: As they were significantly smaller than any wavelength considered, the scattered field is well-approximated by a dipole field. The approximately constant shape of the angular intensity distributions meant that the fraction of scattered light being collected by the objective would also be approximately constant over the measured spectral range.

For the larger JPs, the comparison of measured and simulated spectra would necessitate a correction for the differing distributions.

[1] TO DO: serial number

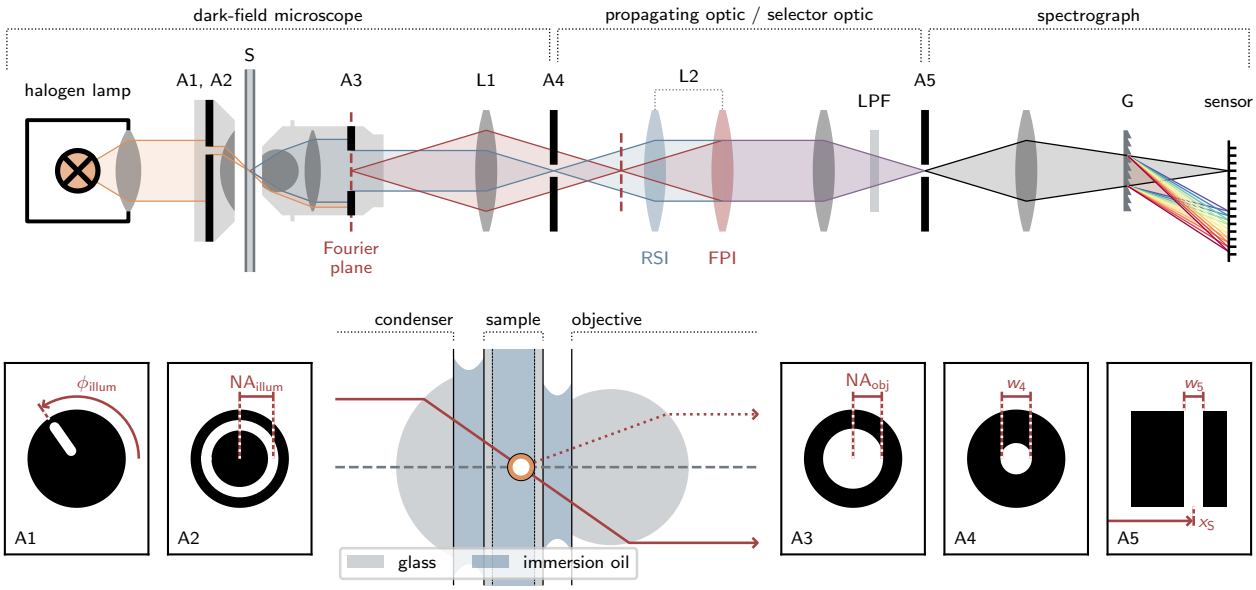

Figure 1: (top) Imaging light path. In the immediate surroundings of the particle under observation **(bottom center)**, the ambient refractive index is virtually homogenous, due to the usage of immersion oil inside the sample. Schematics of the apertures (**A1**-**A5**) are shown below. A4 lies in an image plane, A1-A3 lay in Fourier planes. Depending on the placement of L2, either the image plane or the Fourier plane may be imaged onto A4, and subsequently the camera sensor.

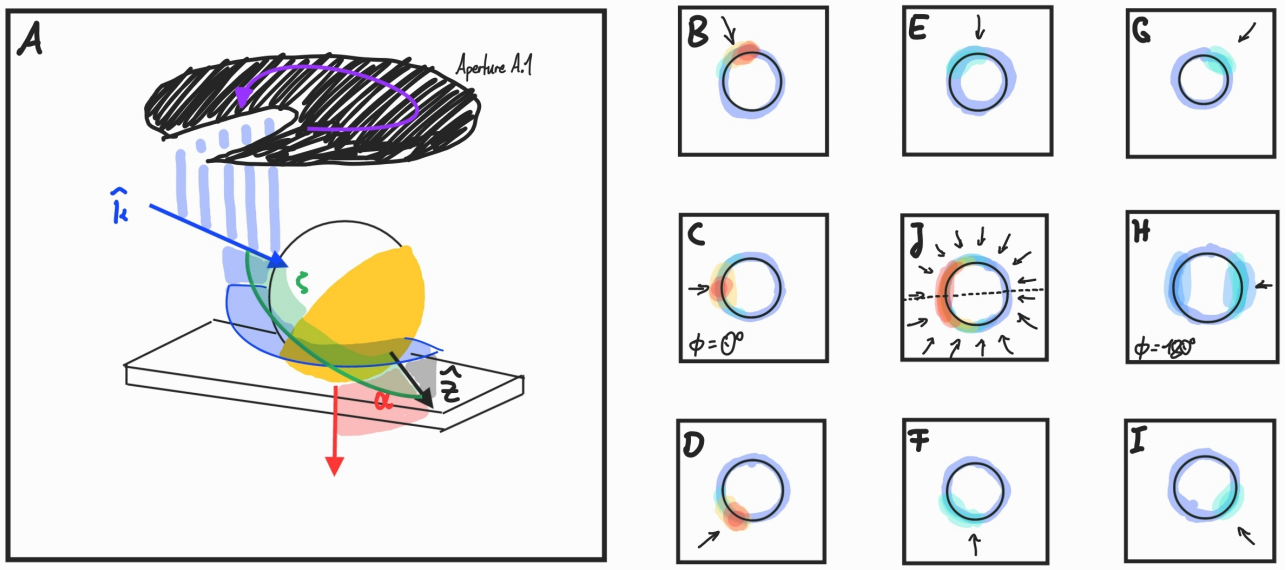

Figure 2: Selective Illumination: **A:** By rotating the aperture A1 the direction of illumination on the particle can be controlled within the range permitted by its out-of-plane orientation. **B-I:** Dark-field images of a JP under restricted illumination. The arrows signify the in-plane angle of the illumination. **J:** The same JP under unrestricted (normal) dark-field illumination.

Finite-Element Simulations

The finite-element simulations were performed in COMSOL Multiphysics 6.1. [Intro to the geometric model. The COMSOL model is qualitatively the same as in [5].] The model geometry, based on models E1 and E2 from [5], was defined in particle-coordinates, i.e. $\hat{z}$ coincides with the z-axis and $\hat{k}$ lies in the x,z plane.

As parameters, the simulation takes in the *illumination angle*,

$$\zeta := \measuredangle\left(\hat{z},\hat{k}\right) ,$$

and the incident (vacuum-) wavelength λ.

For the complex refractive index of gold, the values by Johnson & Christy [10] were used. The medium surrounding the particle was modelled with a refractive index of 1.51 to mimic the immersion oil used in the experiments.

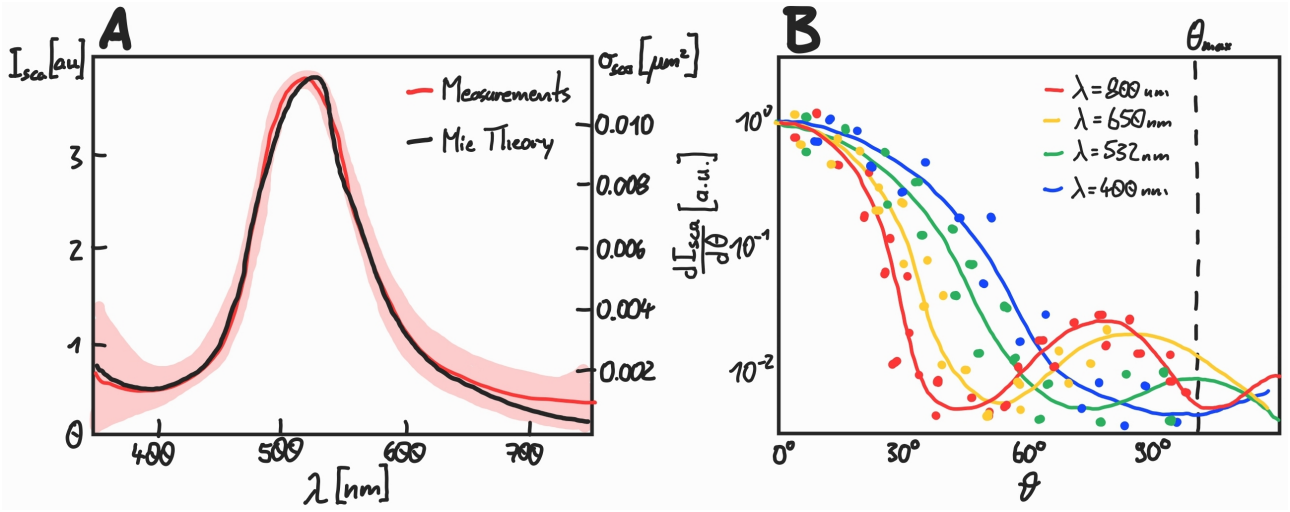

Figure 3: (Placeholder) **A:** Scattering spectrum of 65 nm Au NPs. The shaded area corresponds to the SNR. **B:** Scattering intensity of a spherical Au NP, $d = 250\,\mathrm{nm}$ versus the scattering angle for various wavelengths. The lines show the predictions of GLMT [9], the points show measurement results.

Given a plane wave

$$\vec{E}_{\mathrm{incident}}(\vec{x},t) = \vec{E}_0 \cdot \exp\left(\mathrm{i}\,\vec{k}\cdot\vec{x} - \mathrm{i}\,\omega\,t\right)$$

as the incident field, the solver produced a point-wise solution

$$\vec{E}(\vec{x},t) = \vec{E}_{\mathrm{incident}}(\vec{x},t) + \vec{E}_{\mathrm{sca}}(\vec{x},t)$$

to Maxwell's field equations on the defined geometry, where $\vec{E}_{\mathrm{sca}}(\vec{x},t)$ is the scattered field.

The scattering cross-section of the particle was calculated from the scattered field as

$$\sigma_{\mathrm{sca}} = \frac{2\mu_0\mu_r}{\left\|\vec{E}_0\right\|^2} \cdot \oint_{\partial V} \left\langle \vec{S}_{\mathrm{sca}} \right\rangle_t \cdot \mathrm{d}\vec{A}\,,$$

where $\vec{S}_{\mathrm{sca}}$ is the Poynting vector of the scattered field and $\langle\cdot\rangle_t$ denotes the time average.

[Explanation on how the scattering intensity is resolved for $\hat{k}$] The scattered field can, according to Fourier's theorem, be decomposed into plane-wave components

$$\mathrm{d}\vec{E}(\vec{x},t) := \vec{\mathcal{E}}(\vec{k}) \cdot \exp\left(\mathrm{i}\,\vec{k}\cdot\vec{x} - \mathrm{i}\,\omega\,t\right)\,\mathrm{d}^3k\,,$$

such that $\vec{E}_{\mathrm{sca}} = \iiint_{\mathbb{R}^3} \mathrm{d}\vec{E}$. The amplitudes $\vec{\mathcal{E}}(\vec{k})$ of the components are given by the Fourier transform of $\vec{E}(\vec{x},t)$. The intensities of the components are given by [11, 12]

$$\mathrm{d}\mathcal{I}(\vec{k}) = \frac{\left\langle \left\|\vec{\mathcal{E}}(\vec{k})\right\|^2 \right\rangle_t}{2\mu_0\mu_r}\,\mathrm{d}^3k\,.$$

With any fixed wavelength λ, the wavevectors are conveniently expressed as $\vec{k} = 2\pi\lambda^{-1}\cdot\hat{k}_{\mathrm{sca}}$, where $\hat{k}_{\mathrm{sca}} \in \mathcal{S}^2$ is a unit vector. One obtains the spectral and angular distribution of scattered light, $\mathrm{d}\mathcal{I}(\lambda,\Omega)$, where Ω parametrizes the 2-sphere.

Emulation

In order to be able compare the simulation results to the measurements, the the limited collection angle of the objective has to be taken into account. Thus, while the "true" scattering intensity is the integral over the angular distribution of scattered light,

$$P_{\mathrm{sca}}(\lambda) = \oiint_{\Omega\in\mathcal{S}^2} \mathrm{d}\mathcal{I}(\lambda,\Omega)\,,$$

the measured value corresponds to the integration over a certain angular range $\mathcal{D} \subset \mathcal{S}^2$. Specifically, $\mathcal{D}$ is the interior of a small circle whose angular radius ρ is defined by the numerical aperture of the objective,

$$\rho = \operatorname{asin}\left(\frac{\mathrm{NA}}{n_{\mathrm{medium}}}\right)\,,$$

according to the Abbe sine condition. [13, 14]

[I'm leaving out anything to do with polarization, because I'm only looking at unpolarized measurements and the description of how I define polarization in the simulation and subsequently get rid of it in the emulation feels redundant.]

The measured scattering cross-section of the JP corresponds to the sum of the intensities of all plane-wave components of the scattered field that enter the measurement optics:

$$\sigma_{\mathrm{sca,measured}} \propto \iint_{\mathcal{D}} I\left(\hat{k}'\right)\,\mathrm{d}\Omega\,,$$

Where $\mathcal{D} \subseteq \mathcal{S}^2$ is the set of propagation directions $\hat{k}'$, for which a plane wave component will contribute to the signal on the detector. In the experiment, the requirement is for it to enter the objective, and thus

$$\mathcal{D} = \left\{ \hat{k}' \in \mathcal{S}^2 \;\middle|\; \measuredangle\left(\hat{k}', \hat{o}\right) < \theta_{\mathrm{NA}} \right\}\,,$$

where θ_{NA} is the opening angle of the objective's collection cone, given by the numerical aperture,

$$\theta_{\mathrm{NA}} = \operatorname{asin}\frac{\mathrm{NA}}{n}\,.$$

- The simulation provides values of the scattered field for sampled values of ζ.
- The numerical aperture of the dark-field condenser defines $\measuredangle(\hat{k}, \hat{o})$.
- The out-of-plane angle α of the JP is unknown and not uniquely defined by ζ and $\measuredangle(\hat{k}, \hat{o})$. We sample $\alpha \in [0, \pi]$ and weight the results by $p(\alpha) = \sin\alpha$.[2]

Results

Dark-Field Spectra

Recorded scattering spectra of the JPs are shown in Figure 4B.

[Broad behaviour: Intensity of the scattering signal increases with wavelength.]

All spectra show a sharp upward bend at 500 nm, the same as can be seen in the scattering spectra of similar-sized Au spheres.

The cumulative spectra show an monotonous increase of the scattering intensity over the spectral range up to 950 nm. Beyond, the measured spectra diverge from one another, some dropping off, others continuing the trend of linear increase. [plot] This is an artifact of the signal processing in conjunction with the low efficiency of the setup at wavelengths beyond 1000 nm.

The emulated spectra show the same qualititive behaviour between 500 and 950 nm, though their average[3] derivative is consistently [check!] lower. No obvious features can be resolved in this spectral range. In the NIR, all emulated spectra continue the increasing trend.

Consistent between all measurements, there is a bump at 550 nm. This is, notably, the same wavelength as the main peak of an arbitrarily small AuNP's scattering spectrum.

Dark-Field Spectra, Selective Illumination

[Particle appears much brighter when illuminated from the Au side. It stands to reason that its out-of-plane orientation made it such that when the aperture was rotated such that the PS side would be illuminated, the light *actually* hit side-on. (I.e. cap pointing ca. 30° up towards the condenser)]

With the selective illumination mode, we demonstrate the dependence of the JP's scattering intensity on the propagation direction of the incident light. [need to have another look at the data]

Fourier Plane Spectra

In the multiplexed Fourier plane spectroscopy, the angular distributions of the scattering intensity became visible. We considered three settings of the selective illumination:

- illumination from the Au side, i.e. maximal ζ,
- illumination from the PS side, i.e. minimal ζ and
- side-on illumination, i.e. $\zeta \approx \pi/2$.

For all illumination directions, most of the scattered light is only lightly deflected off of the propagation direction of the incident light. However, there were qualitative distinctions between the distributions that hold over the entire spectral range under consideration: The peak brightness was highest for illumination from the Au side, while a wider peak and significant sideways scattering accumulated into a greater absolute brightness under illumination from the PS side.

Unsurprisingly, the distributions were symmetric about the axis of illumination. This was not the case for the side-on illumination, where light was preferentially scattered in the direction of the Au side.

Numerical Results, Far-Field Patterns

The simulated far-field patterns show the same results.

Numerical Results, Dark-Field Spectra

The measured intensity increase through the visible range coincides with the increase of the scattering cross-section. In the NIR range, the measured brightness increases further; here it is due to the broadening of the forward scattering peak.

For wavelengths beyond 700 nm, the scattering cross-sections, between illumination from the Au side and from the PS side, are virtually the same. They are, moreover, on average significantly larger than that for side-on illumination. However, at $\lambda = 1210$ nm, they have a local minimum where the scattering cross-section is less than that for side-on illumination. This points at a polar plasmon mode that is being excited out-of-phase. [Explain better what I mean.] [Also: I would expect a peak in the absorption cross-section there. Motivate why and check if it's there.]

Numerical Results, Scattering Spectra

Discussion

[We find that the scattering cross-section heavily depends on the orientation of the JP.] Over the spectral range that we analyzed, though decidedly not in

[2] $p(\alpha)$ is the probability density function for the out-of-plane angle of a randomly oriented spherical JP. For the derivation, see the supplementary material.

[3] The average was weighted for the likelihood of the particular out-of-plane orientation of the particle as well as for the NA setting of the objective, both of which influence the integration sub-domain.

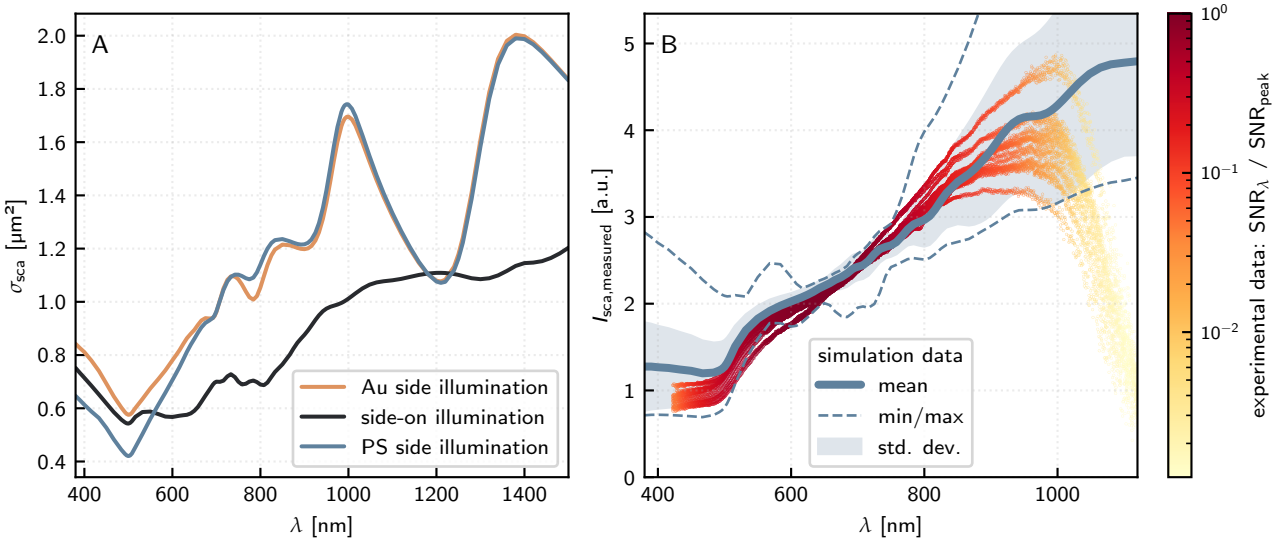

Figure 4: A: simulated scattering spectrum of the JP under illumination from the Au side (yellow), from the PS side (blue) and from the equatorial side (black). **B:** measured scattering spectra (orange) atop value range as determined by simulation + emulation (blue).

general, the scattering efficiency of the particle was ... greater if it was illuminated from either the Au or the PS side than if it was illuminated side-on. In both cases, the scattering spectra have multiple peaks. Between axial and side-on illumination, though, there is no clear correspondence between these peaks.

E.g., for side-on illumination, there is a scattering peak at $\lambda \approx 550\,\text{nm}$, that has no counterpart in the spectra for axial illumination. We ascribe this peak to the nanostructure plasmon resonance of gold: It sits right around that wavelength and it is only under side-on illumination that the incident electric field may be perpendicular to the surface of the Au cap at its points of highest curvature, that being the cap's perimeter.

The bump at $\lambda \approx 550\,\text{nm}$ is discernable in both real and emulated measurements, while only appearing in the raw scattering cross-sections for side-on illumination. Notably, this peak occurs at the same wavelength as the main LSPR for an arbitrarily small AuNP. We reason that this plasmon is excited in the rim of the cap by electric fields that are perpendicular to the Au surface in its regions of maximal curvature.

Conversely, the peak at $\lambda \approx 996\,\text{nm}$ is present under just the opposite circumstances, i.e. when $\hat{k} \parallel \hat{z}$. For these orientations, the system is rotationally symmetric in the polarization average and the surface plasmon propagates along the polar direction on the Au cap, inward for $\zeta = 0$ and outward for $\zeta = \pi$. A quantity akin to a wave vector can be assigned to the polar surface plasmon mode, by counting the sign changes of the surface charge density on a geodesic path from the apex of the cap to its rim. For the 996 nm peaks, this means $\tilde{k} = \pm 3$. [Similarly, we can assign such a pseudo wave vector to all the other peaks in the scattering spectra for axial illumination. The result is Figure 5.]

[Proper analysis of the surface plasmon wavevector stuff.]

Neither of these peaks is present[4] in the scattering spectrum of an equivalently sized Au sphere. This implies that the associated surface plasmon modes do not exist on a closed sphere in this form. [The way the electric fields look, it's due to interference of the outer and inner surface plasmons, so perhaps something similar could be seen on a CoreShell?]

[For side-on illumination but arbitrary polarization, there is also something happening on the cap, not just on the rim. Would that be an extra class of modes? (let's call 'em longitudinal to distinguish them from the polar and azimuthal modes) And are those the tiny peaks in the side-on scattering spectrum between 650 and 850 nm?]

Comparing the angular distributions to those of a Mie particle though, there is clear similarity: Non-global maxima become more well-distinguished and fewer in number as wavelength increases. The same happens as the direction of illumination is changed from $\hat{k} \perp \hat{z}$ to $\hat{k} \parallel \hat{z}$: Both parameter changes can, from a Mie-theoretical point of view, be understood as a decreasing size parameter and thus the transition from the ray optics regime ($\lambda \ll R$) to a dipole model ($\lambda \gg R$).

[The out-of-plane orientation of the JP is not easy to infer: None of the spectral features that signify a specific illumination angle are resolvable. ...] The spectral peaks that are characteristic to each orientation are not recognizeable in a measurement. [how to make them visible?]

[A summary figure of sim results: scattering spectra, Mie plots and the like]

[Discussion about the angular distributions - Lift

[4] discernable?

something from the MA.]

Conclusion & Outlook

In summary, we conducted spectroscopic studies of the light scattering behaviour of individual, micrometre-sized Janus particles. We find that the anisotropy of the JP causes certain features to appear in and disappear from its scattering spectrum under certain orientations, particularly in the NIR range.

The scattering spectrum of the JP is qualitatively different from that of equivalently-sized Au spheres for all directions of illumination, though correspondences between some features exist.

Coarse-grained simulations for longer wavelengths (up to 1400 nm) suggest that the drop-off that was originally inferred in [12] does not manifest in actuality.

An experimental setup that can detect these features, possibly even in real time, is feasible.

Interesting things to do with this in the future might be...

- Direct analysis of the surface plasmons: Decomposition of the tangential electric field in an appropriate basis (vector hemispherical harmonics?) to find relative excitation of every (important) surface plasmon mode, depending on wavelength and illumination angle.
- Real-time spectroscopy to track a JP's out-of-plane angle.

References

1. Bregulla, A. P. & Cichos, F. Flow fields around pinned self-thermophoretic microswimmers under confinement. *J. Chem. Phys.* **151,** 044706. https://doi.org/10.1063/1.5088131 (2019).
2. Auschra, S., Bregulla, A., Kroy, K. & Cichos, F. Thermotaxis of Janus Particles. *Eur. Phys. J. E* **44.** https://doi.org/10.1140/epje/s10189-021-00090-1 (2021).
3. Selmke, M., Khadka, U., Bregulla, A. P., Cichos, F. & Yang, H. Theory for controlling individual self-propelled micro-swimmers by photon nudging I: directed transport. *Phys. Chem. Chem. Phys.* **20,** 10502. https://doi.org/10.1039/c7cp06559k (2018).
4. Ilic, O. *et al.* Topologically enabled optical nanomotors. *Sci. Adv.* **3,** e1602738. https://advances.sciencemag.org/content/3/6/e1602738 (2017).
5. Patzschke, F. H. *Finite Elements Simulations of Optical Torques on Metal-Dielectric Janus Particles* Bachelor's Thesis (Universität Leipzig, 2020).
6. Islam, M. M., Hossen, M. M., Koschny, T. & Hillier, A. C. Shape- and Orientation-Dependent Scattering of Isolated Gold Nanostructures Using Polarized Dark-Field Microscopy. *J. Phys. Chem. C* **125,** 11478–11488. eprint: https://doi.org/10.1021/acs.jpcc.1c03671. https://doi.org/10.1021/acs.jpcc.1c03671 (2021).
7. Mie, G. Beiträge zur Optik trüber Medien, speziell kolloidaler Metallösungen. *Annalen der Physik* **330,** 377–445. https://doi.org/10.1002/andp.19083300302 (3 1908).
8. Bohren, C. F. & Huffman, D. R. *Absoprtion and Scattering of Light by Small Particles* Wiley Professional Paperback Edition, 82–129, 136. ISBN: 978-0-471-29340-8 (John Wiley & Sons, Weinheim, 1998).
9. Gouesbet, G. & Gréhan, G. *Generalized Lorenz–Mie Theories* Second Edition. ISBN: 978-3-319-46873-0 (Springer, Heidelberg, 2017).

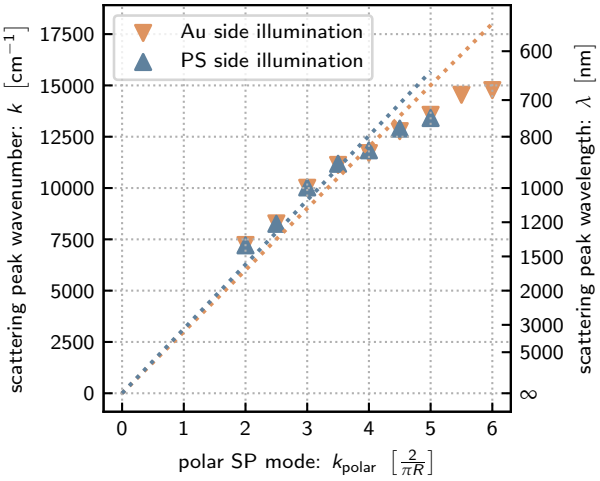

Figure 5: Excitation wavelengths of peaks and valleys in the axial illumination scattering spectra vs. spatial frequency of the electric field on the surface of the Au cap.

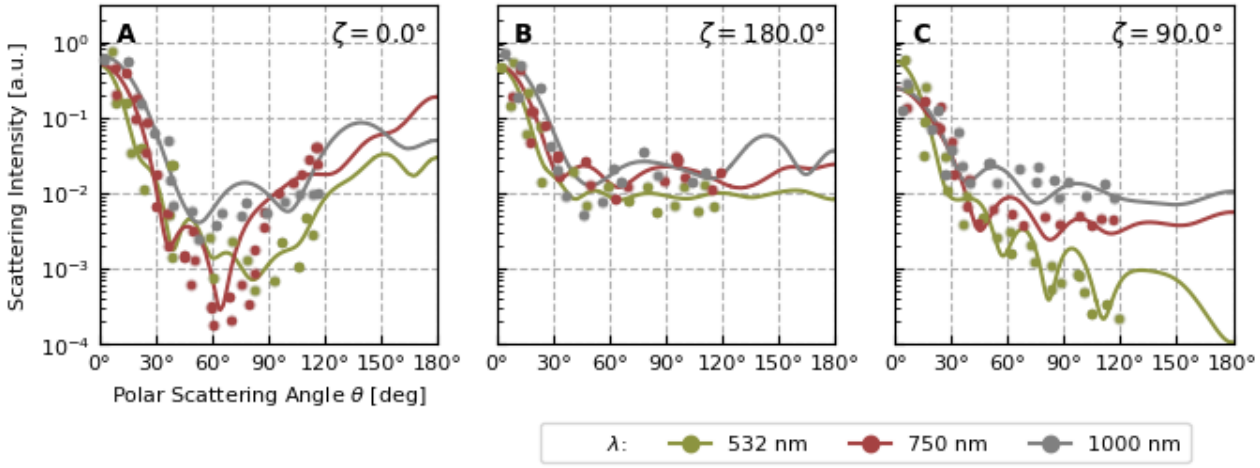

Figure 6: Scattering intensity of the JP versus scattering angle. The points signify measured intensities while the lines are simulation results. **A** and **B** show the cylindrically symmetric cases of illumination from the PS side and from the Au side, respectively, i.e. where $\hat{k} \parallel \hat{z}$. In **C**, the light is incident side-on ($\hat{k} \perp \hat{z}$, $\zeta = \pi/2$). Disregarding the local extrema, qualitatively distinct large-scale behaviour is apparent: Under illumination from the PS side **(A)**, the scattering intensity becomes globally minimal in the sideways direction. Meanwhile, under illumination from the Au side **(B)**, it reaches a plateau and under side-on illumination **(C)**, the scattering intensity drops consistently between forwards and backwards.

10. Johnson, P. B. & Christy, R. W. Optical Constants of the Noble Metals. *Phys. Rev. B* **6,** 4370. `https://doi.org/10.1103/PhysRevB.6.4370` (1972).

11. Griffiths, D. J. *Introduction to Electrodynamics* Fourth edition. ISBN: 978-0-321-85656-2 (Pearson Education, London, 1981).

12. Patzschke, F. H. *Orientation-dependent Spectroscopy of Plasmonic Janus Particles* Master's Thesis (Universität Leipzig, 2023).

13. Wagner, R., Heerklotz, L., Kortenbruck, N. & Cichos, F. Back focal plane imaging spectroscopy of photonic crystals. *Appl. Phys. Lett.* **101,** 081904. `https://doi.org/10.1063/1.4746251` (2012).

14. Wagner, R. & Cichos, F. Fast measurement of photonic stop bands by back focal plane imaging. *Phys. Rev. B* **87,** 165438. `https://doi.org/10.1103/PhysRevB.87.165438` (2013).

Acknowledgements

[...]

Author Contributions

F.C. and F.H.P. designed the experiments; F.H.P. constructed the optical setup, performed the experiments, implemented the simulations and conducted the data analysis; F.H.P. and A.M.A. and wrote the manuscript; All authors reviewed the manuscript.

Competing Interests

The authors have no competing interests to declare.

Additional Information

[...]